ELSEVIER

Nuclear Physics B 450 [FS] (1995) 463–494

NUCLEAR PHYSICS B [FS]

Three-dimensional folding of the triangular lattice

M. Bowick[a], P. Di Francesco[b], O. Golinelli[b], E. Guitter[b]

[a] *Physics Department, Syracuse University, Syracuse, NY 13244-1130, USA*

[b] *CEA, Service de Physique Théorique de Saclay, F-91191 Gif sur Yvette Cedex, France*

Received 22 February 1995; revised 1 June 1995; accepted 2 June 1995

Abstract

We study the folding of the regular triangular lattice in three-dimensional embedding space, a model for the crumpling of polymerised membranes. We consider a discrete model, where folds are either planar or form the angles of a regular octahedron. These "octahedral" folding rules correspond simply to a discretisation of the 3d embedding space as a Face Centred Cubic lattice. The model is shown to be equivalent to a 96-vertex model on the triangular lattice. The folding entropy per triangle $\ln q_{3d}$ is evaluated numerically to be $q_{3d} = 1.43(1)$. Various exact bounds on q_{3d} are derived.

1. Introduction

Polymerised membranes have recently been the object of intense investigation [1], both as natural 2d generalisations of polymers and as models for biological systems. From the theoretical point of view, polymerised membrane models are archetypical examples of the interplay between geometry and statistical mechanics.

In the simplest formulation, one considers only *phantom* membranes, i.e. membranes where steric constraints due to self-avoidance are not taken into account. When embedded in d-dimensional space, the statistical behaviour of such phantom membranes is governed by their bending rigidity. Phantom membranes have been predicted to undergo a geometrical crumpling transition between a low-rigidity crumpled phase and a high-rigidity flat phase. This prediction is based both on various analytic results on continuous models [2–4] and on various numerical simulations [5,6]. The continuous character of the transition, clearly established in sufficiently high embedding space dimension, is still not fully determined in 3d embedding space. A non-trivial corollary of the crumpling transition is the very existence of a stable flat phase at high rigidity, which in turn can only be explained by an anomalous theory of elasticity [7].

SSDI 0550-3213(95)00290-1

The above picture of a crumpling transition is strongly modified by the introduction of steric constraints to describe *self-avoiding* membranes. At the analytic level, the generalisation of the theory of self-avoiding polymers to membranes has attracted much attention [8] and raises in particular the crucial question of the precise status of the theory. At present, the corresponding results have unfortunately not yet reached a suitable level of predictability. On the other hand, many results on self-avoiding polymerised membranes come from various numerical studies based on either Monte Carlo or molecular dynamics methods [9]. All the simulations agree on the fact that the crumpled phase and the crumpling transition should be suppressed by the self-avoidance constraints, the membrane being always in the anomalous flat phase. A crumpled phase seems, however, to be recovered either by going to larger embedding space dimension [10], or by using an inpenetrable plaquette model [11].

As in other domains of random surface physics, the recourse to discrete formulations has proved to be a very powerful approach, with the advantage of permitting direct numerical simulations, as well as leading to exact solutions for particular models. In the simplest discretised version, the polymerised membrane is modelled by a regular triangular lattice with fixed connectivity, embedded in a d-dimensional space. In the above-mentioned numerical references, the lengths of the links of the lattice were allowed to have small variations, either forming "tethers" between hard spheres (as in Ref. [5] where the geometrical 3d crumpling transition was first predicted numerically), or being governed by some confining pair potential (as in molecular dynamics simulations).

In this paper, we shall consider only phantom membranes and use a different approach by taking a discrete model where the lengths of the links of the triangular lattice are *fixed*, say to unity. For such membranes, the only remaining degree of freedom is that of *folding* of the lattice, whose links serve as hinges between neighbouring triangles. Membrane folding was first studied in 2d embedding space, where it can be formulated as an 11-vertex model on the triangular lattice. The entropy of folding, which counts the number of distinct folded states of the lattice in the thermodynamic limit, was first estimated numerically in Ref. [12]. The 2d folding problem was then solved exactly in Ref. [13], through the equivalence with the 3-colouring problem of the links of the triangular lattice [14]. A further study, including a bending rigidity, performed in Ref. [15], led to numerical evidence of a first-order folding transition of the membrane.

In this paper, we address the 3d folding problem, where the embedding space now has 3 dimensions, in an attempt to recover results for tethered membranes in the folding language. In particular the 2d folding transition could be smoothed and lead to a continuous 3d folding transition, analogous to the 3d crumpling transition of phantom membranes. The present work is devoted to a suitable definition of the 3d folding problem, amenable to numerical simulations, and to various reformulations as a vertex model, constrained spin system and colouring problem. We use these formulations to estimate the entropy of 3d folding both numerically and analytically.

The paper is organised as follows. In the first section, we define the general problem of folding of the triangular lattice in embedding space with arbitrary dimension and recall a few results for the case of dimension 2. In Section 3, we define the discrete

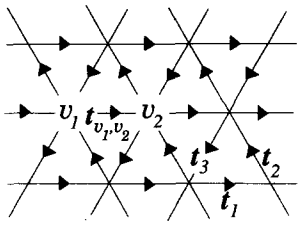

Fig. 1. The oriented triangular lattice: triangles pointing up (resp. down) are oriented counterclockwise (resp. clockwise). The three tangent vectors t_i, $i = 1, 2, 3$, have a vanishing sum in the embedding space.

problem of 3d "octahedral" folding, which corresponds to a discretisation of the 3d embedding space as a Face Centred Cubic lattice. In Section 4, we show that the 3d octahedral folding is equivalent to a 96-vertex model on the triangular lattice. This is done by use of face spin variables defined in Subsection 4.1, which in turn parametrise some generators of the tetrahedral group studied in Subsection 4.2. From the group formulation we derive in Subsection 4.3 the local folding constraints on these face variables, leading to a complete determination of the 96 folding vertices. Section 5 is devoted to the numerical evaluation of the entropy of 3d folding. Various exact bounds on this entropy are derived in Section 6, by re-expressing the 3d octahedral folding problem as a dressed 3-colouring problem (Subsection 6.1), and performing some rough bounding of the partition function (Subsection 6.2). Improved bounds are obtained in Subsection 6.3 by comparison with the 2d folding problem in a field. We discuss in Section 7 our results for the entropy (Subsection 7.1), as well as a natural generalisation of the octahedral folding problem in dimension $d > 3$ (Subsection 7.2). Concluding remarks are gathered in Section 8, and some extensions of Subsection 6.2 are given in Appendix A.

2. The folding rule

A folding in $\mathbb{R}^d$ of the regular triangular lattice is a mapping which assigns to each vertex v of the triangular lattice a position $\boldsymbol{X}_v$ in d-dimensional embedding space $\mathbb{R}^d$, with the "metric" constraint that the euclidean distance $|\boldsymbol{X}_{v_2} - \boldsymbol{X}_{v_1}|$ in $\mathbb{R}^d$ between nearest neighbours v_1 and v_2 on the lattice is always unity. Under such a mapping, each elementary triangle of the lattice is mapped onto an equilateral triangle in $\mathbb{R}^d$. In general, two adjacent triangles form some angle in $\mathbb{R}^d$, i.e. links serve as hinges between triangles and may be (partially) folded. Folding is best described in terms of tangent vectors, which are link variables defined as follows: we first orient the links of the lattice as in Fig. 1, with triangles pointing up (resp. down) oriented counterclockwise (resp. clockwise), and define the tangent vector between two neighbours v_1 and v_2 as the vector

$$\boldsymbol{t}_{v_1,v_2} = \boldsymbol{X}_{v_2} - \boldsymbol{X}_{v_1} \tag{2.1}$$

if the arrow points from v_1 to v_2. The metric constraint states that all tangent vectors have *unit length*. Moreover, with our choice of orientation, the three tangent vectors t_i, $i = 1, 2, 3$, around each face of the lattice must have *vanishing sum*. This is the basic folding rule [1]:

$$t_1 + t_2 + t_3 = 0. \tag{2.2}$$

Up to a global translation in $\mathbb{R}^d$, a folding is therefore a configuration of unit tangent vectors defined on the links of the lattice, obeying the folding rule (2.2) around each triangle.

The two-dimensional ($d = 2$) folding problem of the triangular lattice was addressed in Ref. [13]. It is easy to check that, up to a global rotation in the embedding plane, all the link variables are forced to take their value among a *fixed* set of three unit vectors with vanishing sum. This permits a reformulation of the $d = 2$ folding problem as that of the 3-colouring of the links of the triangular lattice: calling the three fixed vectors blue, white and red, the folding rule translates into the constraint that the three colours around each triangle have to be distinct. This 3-colouring problem was solved by Baxter in Ref. [14] by use of Bethe Ansatz techniques. His result for the thermodynamic partition function measures the number of folding configurations $Z_{2d} \propto q_{2d}^{N_\Delta}$ for a lattice with N_Δ triangles, in the limit of large N_Δ. This gives the folding entropy per triangle $s_{2d} = \ln(q_{2d})$, with [13]:

$$q_{2d} = \frac{\sqrt{3}}{2\pi}\Gamma(\tfrac{1}{3})^{3/2} = 1.20872\ldots. \tag{2.3}$$

The 2d folding problem has also been studied in the presence of bending rigidity, which associates an energy to each folded link, and a magnetic field coupled to the normal vector to the triangles [15]. The system was found to undergo a first-order folding transition. At zero rigidity and zero magnetic field, the lattice is in an entropic folded phase. At sufficiently large rigidity and/or magnetic field, the lattice becomes totally unfolded.

In this paper, we address the case of embedding in $\mathbb{R}^{d=3}$ and, in particular, we are interested in computing the folding entropy s_{3d}.

3. Octahedral folding

In the general 3-dimensional folding problem, the local folding constraint (2.2) imposes only that the three tangent vectors around each face be in the same plane and have relative angles of $2\pi/3$. This, however, does not impose any constraint on the *relative* positions of the two planes corresponding to two adjacent faces, which may form some arbitrary continuous angle. As opposed to the 2d case, this then leads to a problem with continuous degrees of freedom.

[1] On the dual hexagonal lattice, whose vertices are at the centers of the triangles, this basic rule translates into a local conservation law at each vertex, reminiscent of the so-called "ice rule" of integrable vertex models.

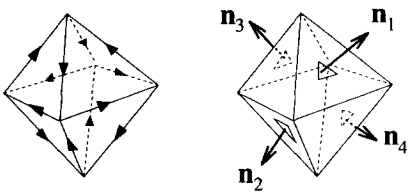

Fig. 2. The oriented octahedron: the edges around each face form triplets of tangent vectors with vanishing sum. The four normal vectors n_i, $i = 1, 2, 3, 4$, are represented on the corresponding outward oriented faces.

Here we wish instead to define some *discrete* model of folding in 3d, in which only a *finite* number of relative angles are allowed between adjacent faces. More specifically, we shall also impose that the link variables themselves take their values among a *finite* set of tangent vectors, now in $\mathbb{R}^3$. For symmetry reasons, we will take this set of tangent vectors to be the (oriented) edges of a regular solid of $\mathbb{R}^3$, made of equilateral triangles only.

There are only three regular solids in $\mathbb{R}^3$ made of equilateral triangles: the tetrahedron, the octahedron and the icosahedron. The edges of the tetrahedron (resp. icosahedron), however, cannot be consistently oriented in order for the corresponding tangent vectors to satisfy (2.2) around each face. This is because each vertex is surrounded by an odd number 3 (resp. 5) of triangles. There is no such problem for the octahedron, as shown in Fig. 2. The 12 links of the octahedron are oriented consistently to form 8 triplets of tangent vectors with vanishing sum corresponding to the 8 faces of the octahedron. From now on, we shall therefore consider the restricted 3d "octahedral folding" problem, where the tangent vectors are chosen from the set of the 12 edge vectors of a regular oriented octahedron. In the folding process, the folding rule (2.2) imposes that the three links of a given face on the original triangular lattice are mapped onto one of the 8 triplets of tangent vectors above. For a given triplet, the triangle can still be in 3! states corresponding to the 3! permutations of the three edges. Each triangle can therefore be in one of $48 = 8 \times 6$ states.

The 8 faces of the octahedron can be labelled as follows: we consider for each face its normal vector, pointing outwards or inwards according to the orientation of its tangent vectors on the octahedron (see Fig. 2). There are four outward oriented and four inward oriented faces which alternate on the octahedron. The normal vectors to opposite faces are equal. This thus defines a set of only four vectors $\boldsymbol{n}_1$, $\boldsymbol{n}_2$, $\boldsymbol{n}_3$ and $\boldsymbol{n}_4$, furthermore satisfying the sum rule $\boldsymbol{n}_1 + \boldsymbol{n}_2 + \boldsymbol{n}_3 + \boldsymbol{n}_4 = \boldsymbol{0}$. Each face is labelled by its orientation (outward or inward) and its normal vector (1, 2, 3 or 4). Notice that, by labelling the normal vectors, we can arbitrarily fix one of the two possible chiralities of the octahedron in this construction. We choose the one corresponding to Fig. 2.

The 12 oriented edge vectors of the octahedron are actually identical to the 6 edge vectors of a tetrahedron, now taken with the two possible orientations. The four normal vectors above are also the normals to this tetrahedron. For each folding map, the image of the folded lattice in $\mathbb{R}^3$ lies therefore on a 3d Face Centred Cubic (FCC)

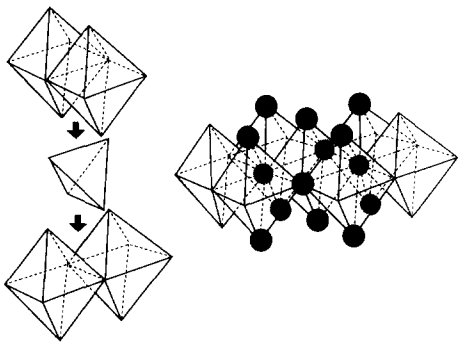

Fig. 3. The Face Centred Cubic lattice viewed as a packing of 3d space with octahedra and tetrahedra.

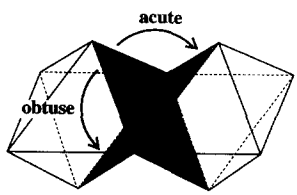

Fig. 4. The four possible folding angles between two adjacent triangles. The neighbour of the dark triangle may (i) be itself on top of the dark triangle (complete fold), (ii) occupy the symmetric position in the same plane (no fold), (iii) lie on the same octahedron (i.e. form an obtuse angle) or (iv) lie on the same tetrahedron (i.e. form an acute angle).

lattice, which consists of a filling of space by octahedra complemented by tetrahedra, as shown in Fig. 3. In this respect, the "octahedral folding" problem simply corresponds to discretising the embedding space as a FCC lattice.

Note finally that nothing prevents the lattice from intersecting itself, hence our construction describes a phantom membrane. The introduction of self-avoidance would result in much more elaborate non-local constraints, far beyond the scope of the present study.

4. 96-vertex model

When stated in terms of tangent vectors, the 3d "octahedral folding" problem involves three types of constraints: face, link and vertex constraints. The first constraint, around each *face*, imposes that the three tangent vectors of a given triangle form one of the 8×6 (ordered) triplets with vanishing sum. The second constraint, on each *link*, arises because two adjacent triangles share a common tangent vector. Given the state of one triangle, any adjacent triangle has one of its tangent vectors already fixed and thus is left with only $4 = 48/12$ possible states. They correspond simply to the four values for the relative angle between two neighbouring triangles, i.e. the angle between the normal

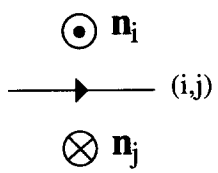

Fig. 5. The labelling (i, j) of an edge of the octahedron, $1 \leqslant i \neq j \leqslant 4$, according to the adjacent normal vectors.

vectors, depicted in Fig. 4. These four values are 0 (no fold: the triangles are side by side), 180° (complete fold: the triangles are on top of each other), $\arccos(-\frac{1}{3}) \sim 109°28'$ (fold with acute angle: the two triangles lie on the same tetrahedron) and $\arccos(\frac{1}{3}) \sim 70°32'$ (fold with obtuse angle: the triangles lie on the same octahedron). Finally, there is a third constraint on the six successive folds around each *vertex* of the lattice: after making one loop, the same tangent vector must be recovered. Since the "metric constraint" is local, there are actually no constraints other than these three (face, link and vertex) constraints.

In the study of the 2d folding problem, i.e. of the 3-colouring problem, the face and link constraints are taken into account by going to $\mathbb{Z}_2$ spin variables σ_i defined on the faces of the lattice. Ordering the colours cyclically, the spin is $+1$ (resp. -1) if the colour increases (resp. decreases) from one link to the neighbouring one on the triangle, oriented counterclockwise. In this language, the actual folds take place exactly on the domain walls of the spin variable. Instead of having a $\mathbb{Z}_3$ colour variable per link, one is left with a $\mathbb{Z}_2$ spin variable per triangle. The vertex constraint translates into a constraint on the six spins $\sigma_1, \ldots, \sigma_6$ around each vertex of the lattice, namely that $\sum_{i=1}^{6} \sigma_i = 0 \bmod 3$. This leads to 22 possible local spin configurations around each vertex, or equivalently, after removing the global $\mathbb{Z}_2$ degeneracy of reversal of all spins, to an 11-vertex model on the lattice [13].

In this section, we shall proceed in the same way for the 3d "octahedral folding" and account for the face and link constraints by expressing folded configurations in terms of two $\mathbb{Z}_2$ variables on the triangles. These variables will indicate the relative states of successive links around the face. We shall then count the number of allowed hexagonal configurations around a vertex: we will find that our problem is now expressible as a 96-vertex model. These vertices and the corresponding rules on the $\mathbb{Z}_2$ variables will be identified in the next section.

4.1. Face variables and counting of the vertices

Let us label the 12 edges of the octahedron as follows: each edge is shared by two adjacent faces, one outward and one inward oriented (see Fig. 2). We label the edges by the indices (i, j), $1 \leqslant i \neq j \leqslant 4$, when the normal vector for the outward face is $\boldsymbol{n}_i$ and the one for the inward face is $\boldsymbol{n}_j$. This convention is illustrated in Fig. 5. There are 12 such couples (i, j). The unit tangent vector associated with the link (i, j) is given by

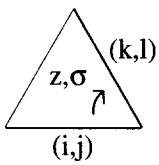

Fig. 6. The transition from a link (i,j) to a subsequent link (k,l) is described by the two $\mathbb{Z}_2$ face variables z and σ.

Table 1
The relative folding state of two neighbouring triangles according to their relative values of z and σ

z_2/z_1	σ_2/σ_1	angle
1	1	no fold
1	−1	complete fold
−1	1	acute fold
−1	−1	obtuse fold

$$\boldsymbol{t}_{(i,j)} = \frac{3}{2\sqrt{2}}\boldsymbol{n}_i \times (-\boldsymbol{n}_j). \tag{4.1}$$

Consider now an elementary triangle of the lattice. Starting from one of its links (i,j) the subsequent link (k,l) counterclockwise must share a face with (i,j) on the octahedron (see Fig 6). This leads to the 4 following possibilities, labelled by the $\mathbb{Z}_2$ face variables $z, \sigma \in \{\pm 1\}$:

$$\begin{aligned} &z = +1 : (i,j) \to (i,l), l \neq j, \quad \epsilon_{ijl} = -\sigma = \pm 1 \\ &z = -1 : (i,j) \to (k,j), k \neq i, \quad \epsilon_{ijk} = +\sigma = \pm 1, \end{aligned} \tag{4.2}$$

where $\epsilon_{ijk} = \sum_l \epsilon_{ijkl}$ is defined in terms of the totally antisymmetric tensor ϵ_{ijkl}, equal to the signature of the permutation $(ijkl)$ of (1234). The value $z = +1$ (resp. $z = -1$) indicates that the two tangent vectors share an outward oriented (resp. inward oriented) face on the octahedron. The spin variable σ takes the value $+1$ (resp. -1) if (k,l) follows (resp. precedes) (i,j) on their common (oriented) face of the octahedron. Using (4.1), one can check that the variable σ also indicates whether the normal vector to the triangle (in the embedding space $\mathbb{R}^3$) is parallel ($\sigma = +1$) or antiparallel ($\sigma = -1$) to the corresponding normal vector of the octahedron.

Considering now two neighbouring triangles, the 4 possible relative values z_2/z_1 and σ_2/σ_1 indicate which type of fold they form, with the correspondence displayed in Table 1. The domain walls for the z variable are the location of the folds which are either acute or obtuse, whereas those for the σ variable are the location of the folds which are either complete or obtuse. The superposition of these two types of domain walls fixes the folding state of all the links, specifying the folding state of the lattice up to a global orientation.

The use of z and σ variables instead of the 12 (i,j) variables incorporates the face and link constraints. Like in the 2d case, the vertex constraint is more subtle and will

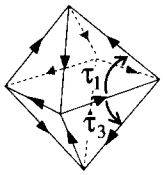

Fig. 7. The action of the generators τ_1 and τ_3 of the tetrahedral group A_4 on a particular edge of the oriented octahedron. All the edges of the octahedron are equivalent, and τ_1 and τ_3 act simultaneously on all the edges according to the same picture.

be studied in the next subsection. Nevertheless, we can easily count at this stage the number of possible configurations around a vertex satisfying this constraint, i.e. the number of possible folded states of an elementary hexagon. Indeed the mapping (4.2) may be represented by a 12×12 connectivity matrix $M_{(i,j),(k,l)}$ with $i \neq j$ and $k \neq l$:

$$M_{(i,j),(k,l)} = \delta_{ik} + \delta_{jl} - 2\,\delta_{ik}\delta_{jl}. \tag{4.3}$$

This matrix acts as a transfer matrix between two successive internal links of the hexagon. The number of configurations of a hexagon is simply given by:

$$\mathrm{Tr}(M^6) = 4608, \tag{4.4}$$

where the trace guarantees that the same link variable is recovered after one loop. These 4608 configurations count as distinct all the foldings which are related by a global change of orientation of the hexagon in embedding space. The order of the resultant degeneracy is 48, corresponding to 12 choices for the first tangent on the octahedron times 4 for the choice of the second from among its 4 neighbours (this latter choice corresponds to the 4 choices of the z and σ variables on the corresponding triangle). This leaves us with $4608/48 = \mathbf{96}$ distinct configurations.

The above computation is also equivalent to counting the number of closed paths of length 6 on the cuboctahedron, i.e. the solid whose vertices sit at the centers of the edges of the octahedron, and whose connectivity matrix is given by (4.3).

4.2. The tetrahedral group A_4

In order to derive the vertex constraints for the z and σ variables around any vertex of the lattice, we will use a group formulation of (4.2). We note here that the 12 links of the octahedron may be uniquely labelled by the even permutations of the set $1,2,3,4$. Indeed the link (i,j) is equivalently represented by the even permutation $(ijkl)$, with $\epsilon_{ijkl} = 1$. With this labelling the alternating group A_4, the group of even permutations of four elements, also known as the tetrahedral group, acts on the space of links. In other words, each element of A_4 is a one-to-one mapping of the set of links onto itself. A fixed element of A_4 acts on a given link by permutation of the four link labels. The order of A_4 is $4!/2 = 12$. These 12 elements map a given link to exactly the 12 links of the octahedron. The group A_4 can be generated by two elements τ_1 and τ_3 defined as:

$$\tau_1 = (243),$$
$$\tau_3 = (134) \tag{4.5}$$

and corresponding to the two elementary mappings shown in Fig. 7. Here we use the standard notation for permutations, by listing their cycles not reduced to one element (e.g. (243) is the permutation $(1234) \to (1423)$, whereas $(12)(34)$ is the permutation $(1234) \to (2143)$). In terms of these generators the 12 elements of A_4 are:

$$\begin{aligned}
e &= \tau_1^3 = \tau_3^3 = \text{identity},\\
\tau_1 &= (243),\\
\tau_3 &= (134),\\
\tau_2 \equiv \tau_1^2 &= (234),\\
\tau_4 \equiv \tau_3^2 &= (143),\\
\tau_1\tau_3 &= (132),\\
\tau_3\tau_1 &= (124),\\
\tau_1^2\tau_3^2 &= (142),\\
\tau_3^2\tau_1^2 &= (123),\\
g \equiv \tau_1\tau_3^2 = \tau_3\tau_1^2 &= (14)(23),\\
d \equiv \tau_1^2\tau_3 = \tau_3^2\tau_1 &= (13)(24),\\
f \equiv \tau_1\tau_3\tau_1 = \tau_3\tau_1\tau_3 &= (12)(34).
\end{aligned} \tag{4.6}$$

Any other sequence of τ_1 and τ_3 can be reduced to one of the above elements by use of the four relations[2]

$$\begin{aligned}
\tau_1^3 = \tau_3^3 &= \text{identity},\\
\tau_1^2\tau_3 &= \tau_3^2\tau_1,\\
\tau_1\tau_3\tau_1 &= \tau_3\tau_1\tau_3.
\end{aligned} \tag{4.7}$$

These relations can be easily understood graphically by following the successive images of a link around the octahedron (see Fig. 7).

4.3. *Vertex rules*

Starting from the link, say (i, j), the four choices of subsequent link (4.2) correspond to the application of the four operators τ_1, τ_2, τ_3 or τ_4, with the correspondence given in Table 2. A folding of an elementary hexagon of the regular triangular lattice corresponds to a product of six basic group elements $\tau_\alpha, \alpha \in \{1,2,3,4\}$, chosen from the four operators above, and such that

$$P \equiv \tau_{\alpha_6}\tau_{\alpha_5}\tau_{\alpha_4}\tau_{\alpha_3}\tau_{\alpha_2}\tau_{\alpha_1} = e. \tag{4.8}$$

[2] These relations also imply that $\tau_1\tau_3^2 = \tau_3\tau_1^2$.

Table 2
The correspondence between the z and σ variables and the elements τ of A_4

z	σ	group element
1	1	τ_1
1	−1	τ_2
−1	1	τ_3
−1	−1	τ_4

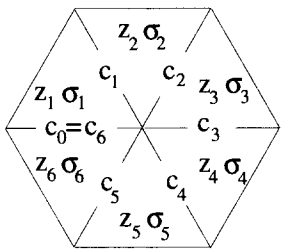

Fig. 8. The six z_i and σ_i variables around a given vertex, and the colours c_i of the interior links.

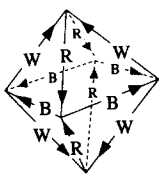

Fig. 9. The assignment of colours for the edges of the octahedron. The four edges of a given colour lie in the same plane. The three colours around a face are distinct.

Let us now translate this constraint into folding rules on the six z and σ variables around each vertex (see Fig. 8). A first folding rule involves the σ variable alone. It ensures the 3-colourability of the links of the triangular lattice in the following way. Let us assign one of three colours (0=blue (B), 1=white (W) or 2=red (R)) to each link of the octahedron. Choosing the colour of link (1342) to be say, 0 (blue), the colour of a link ($ijkl$) is obtained by counting the total number of τ_1 and τ_3 operators required to reach this link from (1342). The colour is this number modulo 3. Since the use of relations (4.7) preserves the total number of τ_1 plus τ_3 mod 3, the colour is well-defined. This is illustrated in Fig. 9: there are 4 blue (resp. white, red) edges lying in the same plane; the three edges have distinct colour around each face. Each folding of the triangular lattice induces therefore a 3-colouring of its links. Conversely, a given 3-colouring of the triangular lattice does not specify its 3d folding state entirely since the same colour may correspond to 4 distinct edges of the octahedron.

The 3-colourability requirement still leads to a first constraint on the σ variables around each vertex: the total number of τ_1 and τ_3 mod 3 in the product P (where we substitute $\tau_2 = \tau_1^2$ and $\tau_4 = \tau_3^2$) must be a multiple of 3. Now in the assignment of colours τ_1 and τ_3 count for 1, while $\tau_2 = \tau_1^2$ and $\tau_4 = \tau_3^2$ count for $2 \equiv -1$ mod 3. Since

this corresponds precisely to their respective values of σ, we find the *first folding rule*:

$$\sum_{i=1}^{6} \sigma_i = 0 \bmod 3 \tag{4.9}$$

for the six spins around the central vertex of the hexagon. As mentioned before, this rule first emerged in the 2d folding problem in Ref. [13], where it also guaranteed the 3-colourability of the triangular lattice.

In contrast with the 2d situation, the restriction (4.9) is not the only constraint here. It only ensures that the product P is one of the four colour-preserving elements e, d, g or f of (4.6). On the other hand, any sequence of τ_1 and τ_3 satisfying (4.9) may be naturally written as a product of e, d, g and f operators by simply regrouping the τ's into triplets. It can be checked that e, d, g and f form a $\mathbb{Z}_2 \times \mathbb{Z}_2$ subgroup of A_4 with the representation

$$\begin{aligned} e &= \tau_1^3 = \tau_3^3 = (1,1), \\ g &= \tau_1\tau_3^2 = \tau_3\tau_1^2 = (\eta,1), \\ d &= \tau_1^2\tau_3 = \tau_3^2\tau_1 = (1,\chi), \\ f &= \tau_1\tau_3\tau_1 = \tau_3\tau_1\tau_3 = (\eta,\chi), \end{aligned} \tag{4.10}$$

where $\eta^2 = \chi^2 = 1$. For the product P to be the identity e, we need the number of η and the number of χ in this decomposition to be separately even. Consider the product P written as a sequence of τ_1 and τ_3 operators and mark the spaces between τ's by 0, 1 or 2 consecutively:

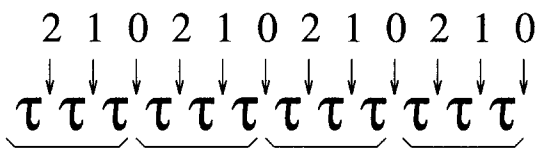

The number of η (resp. χ) is the number of changes from τ_1 to τ_3 or τ_3 to τ_1 occurring at the spaces labelled by 2 (resp. 1). This follows directly from (4.10). On the hexagon these changes can occur *only* at the border between two neighbouring triangles i.e. on interior links. The position of a change (0, 1 or 2) is then simply the colour of the link at which it occurs. In terms of σ variables, the colour c_i of the internal link $i, i = 1, \ldots, 6$, is given by

$$c_i = c_0 + \sum_{j=1}^{i} \sigma_j \bmod 3 \tag{4.11}$$

(the first folding rule (4.9) ensures that $c_6 = c_0$). The quantity $\frac{1}{2}(1 - z_i z_{i+1})$ is 0 or 1 depending on whether or not a change occurs at link i (with the convention $z_7 = z_1$). Defining

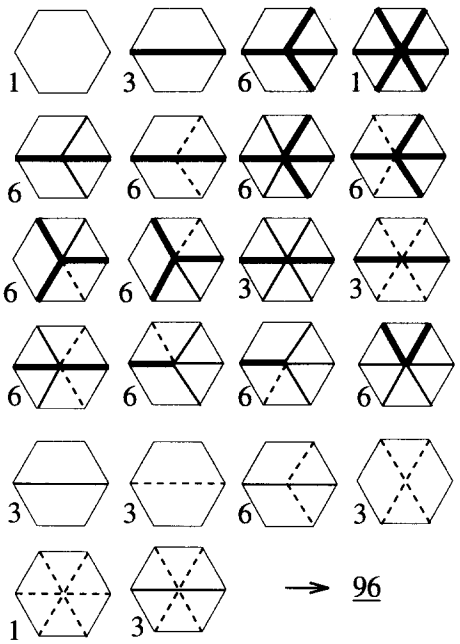

Fig. 10. The 96 vertices satisfying the two folding rules (4.9) and (4.13): no line corresponds to no fold, a thick line corresponds to a complete fold, a thin line corresponds to a fold with obtuse angle and a dashed line corresponds to a fold with acute angle. The degeneracy of each vertex under cyclic permutations of the links is indicated.

$$\alpha_c \equiv \sum_{i=1}^{6} \tfrac{1}{2}(1 - z_i z_{i+1})\delta(c_i, c \bmod 3) \tag{4.12}$$

as the total number of changes on the links of colour c, α_c must be even. This gives the *second folding rule*

$$\alpha_c = 0 \bmod 2 : \quad c = 1, 2. \tag{4.13}$$

Note that (4.13) implies that $\alpha_0 = 0 \bmod 2$ since $\alpha_0 + \alpha_1 + \alpha_2 = 0 \bmod 2$, as the total number of changes between τ_1 and τ_3 is even by cyclicity.

To understand this second folding rule, we first note that a change from τ_1 to τ_3, or vice versa, corresponds to a switch to another face of the octahedron, therefore crossing one of the blue, white or red edge planes bisecting the octahedron (see Fig. 9). The requirement of returning to the *same* (say blue) link after 6 steps is then equivalent to that of crossing each of the white and red planes an even number of times. Indeed α_1 (resp. α_2) is simply the number of crossings of the white (resp. red) plane.

The two folding rules (4.9) and (4.13) are equivalent to the condition (4.8) and therefore characterise the vertex constraint entirely.

With the two folding rules (4.9) and (4.13) we find $384 = 96 \times 4$ vertex configurations (there is a 4-fold global degeneracy under reversal of z or σ), as predicted by our

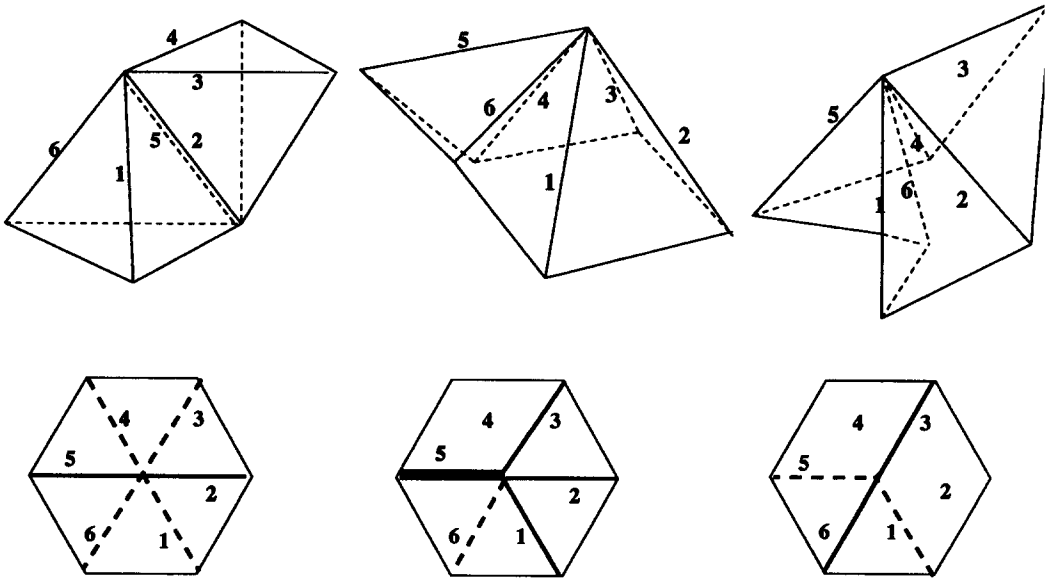

Fig. 11. Examples of 3d octahedral foldings of an elementary hexagon and the corresponding vertices of Fig. 10.

previous counting. The 96 folding vertices are displayed in Fig. 10 with the following conventions: no line corresponds to no fold; a thick line corresponds to a complete folding (180°, flip of σ only); a thin line corresponds to a fold with obtuse angle ($\arccos(\frac{1}{3}) \sim 70°32'$ between normal vectors, flip of both σ and z) and finally a dashed line corresponds to a fold with acute angle ($\arccos(-\frac{1}{3}) \sim 109°28'$, flip of z only). The degeneracy of each vertex under cyclic permutations of the links is also indicated. In Fig. 11 we display a few examples of vertices and the corresponding foldings in 3d space.

The 3d octahedral folding problem is now represented as a 96-vertex model with the vertices of Fig. 10.

5. Entropy: numerical calculation

In this section, we use the above folding rules to estimate numerically the 3d folding entropy per triangle $s_{3d} = \ln q_{3d}$.

The partition function for a parallelepiped of $2L \times M$ triangles, also conveniently thought of as a rectangle of $L \times M$ squares divided into two triangles along one diagonal, can be written as

$$Z_{L,M} = \mathrm{Tr}\ \mathcal{T}(L)^M \tag{5.1}$$

in terms of a row to row transfer matrix $\mathcal{T}(L)$.

The above re-expression of the folding problem in terms of two face variables, the spins $z, \sigma = \pm 1$, enables us to write the transfer matrix from a row of $2L$ triangles to another as a $16^L \times 16^L$ matrix (there are 4 spin configurations (z, σ) on each of the $2L$ triangles). We choose for instance to apply free boundary conditions on the right and left sides of the rectangle. The entries of the row to row transfer matrix read

$\mathcal{T}(L)_{\{z,\sigma\},\{z',\sigma'\}} =$

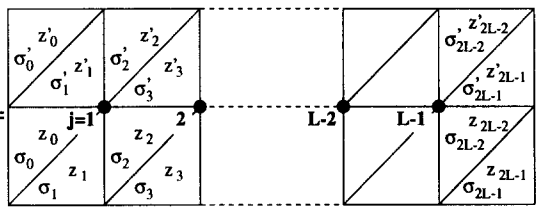

$$= \prod_{j=1}^{L-1} U_j \times V_j, \tag{5.2}$$

where U_j and V_j respectively impose the first and second folding rules (4.9)–(4.13) around each inner vertex j, namely

$$\begin{aligned} U_j &= \delta(\sigma_{2j-2} + \sigma_{2j-1} + \sigma_{2j} + \sigma'_{2j-1} + \sigma'_{2j} + \sigma'_{2j+1}, 0 \bmod 3), \\ V_j &= \prod_{c=1}^{2} \delta(\alpha_c(z_{2j}, z_{2j-1}, z_{2j-2}, z'_{2j-1}, z'_{2j}, z'_{2j+1}), 0 \bmod 2) \end{aligned} \tag{5.3}$$

with $\alpha_c(z_1, z_2, z_3, z_4, z_5, z_6)$ defined by Eq. (4.12). Note that V_j also depends implicitly on the σ's around the vertex j.

In the large-M limit, the partition function (5.1) is dominated by the largest eigenvalue λ_L of the transfer matrix $\mathcal{T}(L)$ and the corresponding free energy per row reads

$$-\lim_{M\to\infty} \frac{1}{M} \ln Z_{L,M} = -\ln \lambda_L. \tag{5.4}$$

The thermodynamic entropy per triangle of the 3d folding problem is therefore

$$s_{3d} = \lim_{L\to\infty} \frac{1}{2L} \ln \lambda_L \equiv \ln q_{3d}. \tag{5.5}$$

The numerical calculation of λ_L is simplified by the fact that $\mathcal{T}(L)$ is a sparse matrix, with entries 0 or 1. Actually the total number N_L of non-vanishing elements of $\mathcal{T}(L)$ reads

$$N_L = \sum_{\{\sigma,z\},\{\sigma',z'\}} \mathcal{T}(L)_{\{z,\sigma\},\{z',\sigma'\}} = \mathrm{Tr}\left(\mathcal{J}[\mathcal{T}(2)]^L\right), \tag{5.6}$$

Table 3
The number N_L of non-vanishing transfer matrix elements and the maximum eigenvalue λ_L for strips of width $L = 1, 2, 3, \ldots, 6$. The ratio $(\lambda_L/\lambda_{L-1})^{1/2}$ is less sensitive to finite size effects than $\lambda_L^{1/2L}$

L	N_L	λ_L	$(\lambda_L/\lambda_{L-1})^{1/2}$
1	256	16.0000000000	
2	6144	25.4891252930	1.2621688994
3	153600	44.9037351935	1.3272837214
4	3891200	83.9628811670	1.3674215892
5	98992128	162.6428871867	1.3917905107
6	2521694208	322.3383026700	1.4077917628

where $\mathcal{J}$ is the 256×256 matrix with all entries equal to 1 (see Ref. [15]). For large L, N_L is dominated by the Lth power of the largest eigenvalue λ_2 of $\mathcal{T}(2)$, easily computed numerically (see Table 3), hence[3]

$$N_L \propto (25.48912\ldots)^L \tag{5.7}$$

to be compared with the total number of elements of $\mathcal{T}(L)$, $(256)^L$.

We display the results for the number of non-vanishing elements N_L and the largest eigenvalue λ_L in Table 3.

The entries of the matrix $\mathcal{T}(L)$ are generated by gluing together around a central vertex two transfer matrices of respective sizes $L/2, L/2$ if L is even or $(L-1)/2, (L+1)/2$ if L is odd. In this way, the time used for generating $\mathcal{T}(L)$ becomes comparable to that used for extracting its largest eigenvalue, by iterative applications of $\mathcal{T}(L)$ on a vector, which we normalise at each step (the normalisation factor converges to λ_L). The value $L = 6$ is obtained by applying some extra symmetry arguments to reduce the size of the matrix $\mathcal{T}(6)$. Using the Padé–Shanks transformation [16,17], we extrapolate the values of $(\lambda_L/\lambda_{L-1})^{1/2}$ of Table 3 to get a numerical estimate of the partition function per triangle (5.5). We find

$$q_{3d} \sim 1.43(1). \tag{5.8}$$

6. Dressed 3-colouring and various bounds on the entropy

In this section, we derive exact bounds for the partition function per triangle q_{3d}. For this purpose, we turn back to the initial definition in terms of tangent vector link variables.

6.1. 3d folding as dressed 3-colouring

The link variable of the 3d folding problem takes its values among the 12 tangent vectors to the octahedron of Fig. 2. Let e_1, e_2, e_3 denote the canonical basis of $\mathbb{R}^3$

[3] The largest eigenvalue of $\mathcal{T}(2)$ matches the value $14 + \sqrt{132}$ up to the precision of our calculation.

Table 4
The twelve unit tangent vectors around the faces of the octahedron of Fig. 2. We display the face label, the normal vector to the face (pointing outwards), the three tangent vectors around the face and their respective colour

face	normal vector	tangent	colour
1	$n_1 = \sqrt{\frac{2}{3}}(x_1 + x_2 + x_3)$	$-x_1 + x_2$	B
		$-x_2 + x_3$	W
		$-x_3 + x_1$	R
2	$n_2 = \sqrt{\frac{2}{3}}(x_1 - x_2 - x_3)$	$-x_1 - x_2$	B
		$x_2 - x_3$	W
		$x_3 + x_1$	R
3	$n_3 = \sqrt{\frac{2}{3}}(-x_1 - x_2 + x_3)$	$x_1 - x_2$	B
		$x_2 + x_3$	W
		$-x_3 - x_1$	R
4	$n_4 = \sqrt{\frac{2}{3}}(-x_1 + x_2 - x_3)$	$x_1 + x_2$	B
		$-x_2 - x_3$	W
		$x_3 - x_1$	R

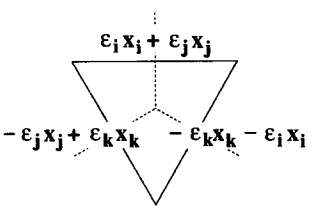

Fig. 12. A typical configuration of tangent vectors around a triangle, expressed in the x basis. Once the colour of each link is chosen, namely the three couples (x_i, x_j), (x_j, x_k) and (x_k, x_i), the three signs ϵ_i, ϵ_j and ϵ_k are still arbitrary.

and let us fix the positions of the 6 vertices of the octahedron to be $(\pm 1/\sqrt{2}, 0, 0)$, $(0, \pm 1/\sqrt{2}, 0)$ and $(0, 0, \pm 1/\sqrt{2})$ in this basis. For instance, the face with normal vector n_1 pointing out in Fig. 2 has the vertices $(1/\sqrt{2}, 0, 0)$, $(0, 1/\sqrt{2}, 0)$, $(0, 0, 1/\sqrt{2})$. Denoting by $x_i = e_i/\sqrt{2}$, $i = 1, 2, 3$, we list in Table 4 the 12 unit tangent vectors grouped according to their outward oriented face label. We also display the colour of each vector, as defined in Fig. 9. In the present language, the colour of a tangent vector simply corresponds to the index of the missing basis vector x modulo 3, i.e. $3 \equiv 0 \rightarrow B$, $1 \rightarrow W$ and $2 \rightarrow R$.

The 48 configurations of tangent vectors around a face of the triangular lattice are specified by the following two sets of data, displayed in Fig. 12:

(i) One of the 6 allowed colourings of the three links, corresponding to a permutation of B, W, R. This specifies for each link the plane x_i, x_j where the tangent vector lies.

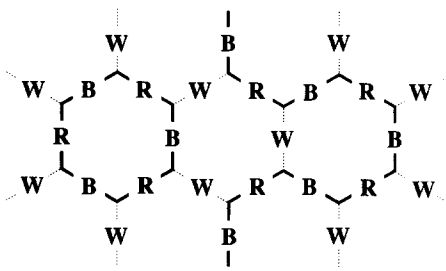

Fig. 13. A sample 3-colouring of the hexagonal lattice: the $BRBR\ldots$ sequences of links form dense loops, represented by thick lines. The coefficient of x_1 in the corresponding tangent vectors can be independently fixed on each loop to be either $+1$ on the B links and -1 on the R links, or -1 on the B links and $+1$ on the R links.

(ii) The assignment of the signs $\epsilon_i, \epsilon_j = \pm$ in the expression of the tangent vector to each link: $\epsilon_i x_i + \epsilon_j x_j$. Due to the folding rule (2.2), each x_i must appear with the two signs, therefore only three signs have to be specified for each triangle, leading to $2^3 = 8$ possibilities.

We recover in this way the $48 = 6 \times 8$ face configurations mentioned above. This presentation has the advantage of decoupling the colouring step (i) from the assignment of signs (ii), therefore displaying the degeneracy of the 3d folding when compared to 3-colouring.

For a given 3-colouring of the links of the triangular lattice, let us now evaluate the number of choices of signs we can make. This is best done on the dual hexagonal lattice, whose vertices are the centers of the faces of the triangular lattice, and whose links (represented by dotted lines in Fig. 12) cross those of the triangular lattice. The tangent vectors are now link variables of the hexagonal lattice. A 3-colouring of the links of the triangular lattice is simply a colouring of the links of the hexagonal lattice, with the constraint that the three links meeting at each vertex have distinct colours. Now a choice of sign, say ϵ_1 for the coefficient of x_1 has to be made on all B and R links. Moreover, this sign propagates from a given B (resp. R) link to the two neighbouring R (resp. B) links, in order for (2.2) to be satisfied at each vertex. More precisely, as shown in Fig. 13, the sequences of B, R, B, R, ... links form closed loops on the hexagonal lattice, and the sign of the x_1 component must alternate along each such loop. For each BR loop, there are two choices of signs of the x_1 components: $\epsilon_1 = +$ (resp. $-$) on all B (resp. R) links of the loop, or conversely. The same holds independently for the choices of signs of the x_2 components along the BW loops and of the x_3 components along the WR loops.

So for a given colouring of the links of the hexagonal lattice, we are left with 2 choices of signs for each of the m_1 BR loops, m_2 BW loops and m_3 WR loops. The partition function for 3d folding reads then

$$Z_{3d} = \sum_{3-\text{colourings}} 2^{m_1+m_2+m_3}, \tag{6.1}$$

where the sum extends over all the 3-colourings of the links of the hexagonal lattice and m_1 (resp. m_2, m_3) denote the number of BR (resp. BW, WR) loops for each colouring. The expression (6.1) identifies the 3d folding problem of the triangular lattice with a dressed 3-colouring problem of the hexagonal lattice, obtained by attaching a $\mathbb{Z}_2$ variable ϵ to each loop of any alternating two colours. Notice finally that the bi-coloured loops above form three *dense* coverings of the hexagonal lattice, in the sense that each vertex of the hexagonal lattice belongs exactly to one BR, one BW and one WR loop. The loops of a given type are *non-intersecting*.

As an exercise let us re-derive the number 96 of vertex configurations in this dressed 3-colouring framework. This number is simply the partition function of a single hexagon H with external legs (dual to an elementary hexagon of the triangular lattice)

$$Z_{\mathrm{H}} = \sum_{3-\text{colourings of } H} 2^{m_1+m_2+m_3}. \tag{6.2}$$

Two situations may occur:

(i) The colouring contains a bi-coloured central loop, in which case one of the m's is equal to 1 and the two others are equal to 3 (open loops), leading to a weight 2^7. There are 6 such colourings.

(ii) All the bi-coloured loops are open. Each external leg belongs to two loops and each loop contains two external legs; the total number of loops is thus equal to the number of external legs 6: this leads to a weight 2^6. There are $6 \times 11 - 6$ such colourings (since the total number of 3-colourings of H is 6×11). We finally get

$$Z_{\mathrm{H}} = 6 \times 2^7 + 60 \times 2^6 = 4608 \tag{6.3}$$

in agreement with (4.4).

6.2. *Simple bounds on the entropy*

The simplest lower bound on

$$q_{3\mathrm{d}} = \lim_{N_\Delta \to \infty} Z_{3\mathrm{d}}^{1/N_\Delta},$$

is obtained by minoration of the sum (6.1) by picking a particular 3-colouring of the hexagonal lattice and evaluating its contribution.

We take the particular configuration depicted in Fig. 14, which maximises m_1, m_2 and m_3 simultaneously. This configuration corresponds to a regular antiferromagnetic ordering of the σ variables. The B and R links are arranged in a dense regular set of hexagonal loops, as well as the B and W links and the W and R links. Since the smallest loop on the hexagonal lattice has length 6, m_1, m_2 and m_3 are clearly maximal. Noticing that the total number N_{H} of hexagons in the hexagonal lattice is equal to the total number $N_{\mathrm{V}} = N_\Delta/2$ of vertices of the dual triangular lattice, this configuration has

$$m_1 = m_2 = m_3 = \tfrac{1}{3} N_{\mathrm{H}} = \tfrac{1}{3} N_{\mathrm{V}} = \tfrac{1}{6} N_\Delta. \tag{6.4}$$

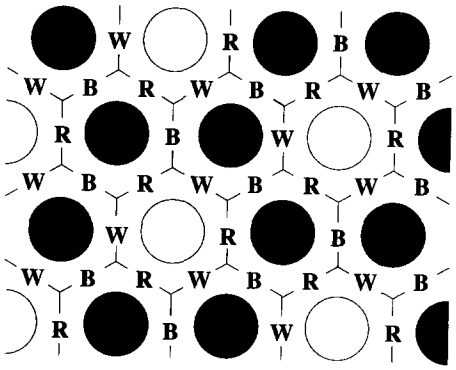

Fig. 14. The antiferromagnetic ground state which maximises m_1, m_2 and m_3 simultaneously. The BR (resp. BW, WR) hexagonal loops are indicated by discs of different colours.

Hence $Z_{3d} > 2^{N_\Delta/2}$, so that

$$q_{3d} \geqslant \sqrt{2} = 1.414\ldots. \tag{6.5}$$

In the 96-vertex language, the contribution of the antiferromagnetic ground state of Fig. 14 corresponds to a restriction of the model to the subset of vertices with alternating σ variables. This subset is characterized by the presence of a thick or a thin solid line on *each* internal link (see Fig. 10). There are $1 + 6 + 3 + 6 = 16$ such vertices. In this respect, $\sqrt{2}$ is simply the exact partition function per triangle of this restricted 16-vertex model, as can be checked directly.

We can improve this bound by incorporating more configurations in our counting, i.e. excitations of the antiferromagnetic ground state of Fig. 14. This is done in Appendix A, leading to the improved lower bound

$$q_{3d} \geqslant 1.429\ldots. \tag{6.6}$$

Using now the fact that, for an arbitrary configuration of 3-colouring of the hexagonal lattice, the numbers m_1, m_2 and m_3 are always smaller than or equal to $N_\Delta/6$, we also get a simple upper bound

$$Z_{3d} \leqslant 2^{N_\Delta/2} \sum_{3-\text{colourings}} 1 = 2^{N_\Delta/2} Z_{2d} \tag{6.7}$$

since the 2d folding problem and that of 3-colouring of the hexagonal lattice are equivalent [13]. Thus, we get an upper bound on q_{3d} in terms of q_{2d} (2.3)

$$q_{3d} \leqslant \sqrt{2}\, q_{2d} = 1.709\ldots. \tag{6.8}$$

6.3. *Improved bounds from 2d folding in a field*

The partition function of the 2d folding problem also has an expansion in terms of *dense* loops on the hexagonal lattice. As mentioned above, the 2d folding problem is

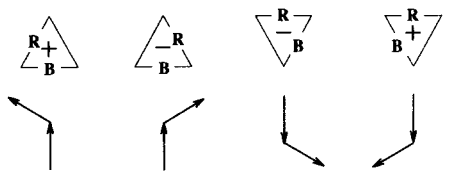

Fig. 15. The four basic possibilities of local orientation for the succession of a B and a R oriented link on the hexagonal lattice (up to global rotation by $\pm 2\pi/3$). The corresponding state of the visited (dual) triangle is represented above each two-link state. The weight in a staggered magnetic field is $e^{h_{st}}$ in the first and third case, and $e^{-h_{st}}$ in the second and fourth ones. The former correspond to left turns, whereas the latter correspond to right turns along the BR loop. Exchanging the B and R links would simply reverse the sign of the face spin σ as well as the orientation of the links.

equivalent to that of 3-colouring of the links of the hexagonal lattice, dual to the original triangular lattice. Instead of considering the 3-colourings of the hexagonal lattice links, however, we can concentrate on say the W-coloured links only. Consider a particular 3-colouring of the links. We have seen above how the paths of $BRBR\ldots$ links form dense, non-intersecting closed loops on the hexagonal lattice. Exchanging the B and R links along any of these loops independently leads to equally admissible 3-colourings of the links. Therefore, for a given *admissible* configuration of W links, one is left with 2 possible independent choices of colourings per BR loop. The number m_1 of such loops is fixed by the position of the W links only. We can write

$$Z_{2d} = \sum_{3-\text{colourings}} 1 = \sum_{W \text{ link config.}} 2^{m_1}. \tag{6.9}$$

This is the 2d version of the 3d folding dense loop expression (6.1).

The solution by Baxter [14] of the 3-colouring problem of the links of the hexagonal lattice includes the introduction of an extra parameter in the weighting of configurations. This parameter may be interpreted as a *staggered magnetic field* h_{st} in the following way. In the language of the face spin (σ) variable ($\sigma = +1$ or -1 on a face indicates whether the colours of adjacent links around the face increase ($B \to W \to R \to B$) or decrease ($B \to R \to W \to B$) counterclockwise), this weight reads

$$\begin{aligned} &e^{\sigma h_{st}} \quad \text{per triangle facing up, } \Delta, \\ &e^{-\sigma h_{st}} \quad \text{per triangle facing down, } \nabla. \end{aligned} \tag{6.10}$$

This gives a maximal weight to the completely folded (antiferromagnetic) ground state of the model (see Fig. 14). Baxter's result is the exact partition function per triangle

$$q_{2d}(h_{st}) = z \prod_{n=1}^{\infty} \frac{(1 - z^{12(1-3n)})}{\sqrt{(1 - z^{12(2-3n)})(1 - z^{12(-3n)})}} \tag{6.11}$$

with $z = e^{h_{st}}$. The above-mentioned result (2.3) for the 2d folding entropy is then recovered in the limit $h_{st} \to 0$, i.e. $z \to 1$.

Let us now translate the result (6.11) into the language of dense BR loops (6.9) on the hexagonal lattice. Consider a particular admissible configuration of W links (a term

in the sum in (6.9)). The extra weights (6.10) can be translated into a dressing of the corresponding BR loops. More precisely, a succession of two B and R links along a BR loop may be in one of the 4 states (up to a rotation by $\pm 2\pi/3$) depicted in Fig. 15. This provides us with a natural orientation of the loops, according to Fig. 15. Each link joins the centers of two adjacent triangles, one pointing up and the other pointing down. We orient the B links toward the upward pointing triangle, and the R links toward the downward pointing triangle. Since triangles pointing up and down alternate along a loop, as well as B and R links, this rule defines a consistent orientation for each BR loop. Reversing the orientation of a loop amounts to exchanging its B and R links, with fixed W links. By inspection of the 4 cases of Fig. 15, we see that the weights (6.10) translate into local weights

$$\begin{aligned} &\mathrm{e}^{h_{\mathrm{st}}} \quad \text{per left turn,} \\ &\mathrm{e}^{-h_{\mathrm{st}}} \quad \text{per right turn} \end{aligned} \tag{6.12}$$

of each oriented BR loop. The previous degeneracy of 2 per loop now amounts to summing over the two orientations of each loop, resulting in a total weight

$$\mathrm{e}^{6h_{\mathrm{st}}} + \mathrm{e}^{-6h_{\mathrm{st}}} = 2\cosh 6h_{\mathrm{st}} \tag{6.13}$$

per loop, as a closed loop has its number of left turns minus its number of right turns equal to ± 6, and the opposite for the opposite orientation. The partition function for the 2d folding problem in a staggered magnetic field reads therefore

$$Z_{2\mathrm{d}}(h_{\mathrm{st}}) = \sum_{W \text{ link config.}} (2\cosh 6h_{\mathrm{st}})^{m_1} \propto q_{2\mathrm{d}}(h_{\mathrm{st}})^{N_\Delta}, \tag{6.14}$$

where the sum is as in (6.9) and $q_{2\mathrm{d}}(h_{\mathrm{st}})$ is defined in (6.11). To get a more symmetric form, we can sum as well over the 3-colourings of the links of the hexagonal lattice, thus removing a factor 2^{m_1} in the above expression, hence

$$\begin{aligned} Z_{2\mathrm{d}}(h_{\mathrm{st}}) &= \sum_{W \text{ link config.}} (\cosh 6h_{\mathrm{st}})^{m_1} \times 2^{m_1} \\ &= \sum_{W \text{ link config.}} (\cosh 6h_{\mathrm{st}})^{m_1} \sum_{B,R} 1 \\ &= \sum_{3-\text{colourings}} (\cosh 6h_{\mathrm{st}})^{m_1}. \end{aligned} \tag{6.15}$$

In the last expression, we could replace m_1 by m_2 or m_3 without distinction.

With this function at hand, we are now ready to give more bounds on $q_{3\mathrm{d}}$. Starting from a given 3-colouring configuration of the dense loop expression (6.1), let us examine the numbers m_1, m_2 and m_3 in more detail. A given BR loop is called *direct* (resp. *indirect*) iff its total weight (6.12) is $\mathrm{e}^{6h_{\mathrm{st}}}$ (resp. $\mathrm{e}^{-6h_{\mathrm{st}}}$). We can therefore decompose the number m_1 of BR loops into the numbers d_1 and i_1 of direct and indirect BR loops respectively. Analogously, we can define the numbers d_2, d_3, i_2, i_3 of direct and indirect BW and WR loops. We have the following relations:

$$m_j = d_j + i_j, \quad j = 1,2,3,$$
$$d_1 - i_1 = d_2 - i_2 = d_3 - i_3. \tag{6.16}$$

To prove the last identity, we note that for a fixed 3-colouring, the total weight (6.10) can be evaluated in terms of any of the three systems of dense loops (BR, BW or WR) independently, with the same result

$$\exp\left(h_{\rm st}\left(\sum_{\Delta}\sigma - \sum_{\nabla}\sigma\right)\right) = e^{6h_{\rm st}(d_1-i_1)} = e^{6h_{\rm st}(d_2-i_2)} = e^{6h_{\rm st}(d_3-i_3)}. \tag{6.17}$$

A first lower bound on q_{3d} can be obtained as follows. In the dense loop expression (6.1) of the partition function Z_{3d}, we restrict the sum to the configurations where all the BR loops are direct. For each admissible colouring of the W links, there is exactly one such configuration of B and R links (it corresponds to a particular choice of orientation on each loop). By summing over these states, we get a minoration $Z_{BR}^{\rm dir}$ of Z_{3d}. All these states have by definition $i_1 = 0$, hence $m_1 = d_1$. Using the identities (6.16), we find that

$$m_2 = d_2 + i_2 = (d_2 - i_2) + 2i_2 = d_1 + 2i_2 = m_1 + 2i_2 \geqslant m_1,$$
$$m_3 = d_3 + i_3 = (d_3 - i_3) + 2i_3 = d_1 + 2i_3 = m_1 + 2i_3 \geqslant m_1. \tag{6.18}$$

The partition function can therefore be bounded from below by

$$Z_{BR}^{\rm dir} = \sum_{\substack{W \text{ link config.} \\ \text{all } BR \text{ loops direct}}} 2^{m_1+m_2+m_3} \geqslant \sum_{W \text{ link config.}} 2^{3m_1}. \tag{6.19}$$

The latter is readily identified as the partition function (6.14) of 2d folding in a staggered magnetic field $h_{\rm st}^*$, such that

$$2\cosh 6h_{\rm st}^* = 2^3, \tag{6.20}$$

i.e.

$$h_{\rm st}^* = \tfrac{1}{6}\ln(4+\sqrt{15}). \tag{6.21}$$

Finally, we get the bound

$$q_{3d} \geqslant q_{BR}^{\rm dir} \geqslant q_{2d}(h_{\rm st}^*) = 1.421\ldots. \tag{6.22}$$

If for a given W link configuration, we now take into account *all* the orientations of the BR loops, Eq. (6.18) no longer holds, but we still have the inequalities

$$m_2 = (d_2 - i_2) + 2i_2 = (d_1 - i_1) + 2i_2 = m_1 + 2i_2 - 2i_1 \geqslant m_1 - 2i_1,$$
$$m_3 = (d_3 - i_3) + 2i_3 = (d_1 - i_1) + 2i_3 = m_1 + 2i_3 - 2i_1 \geqslant m_1 - 2i_1, \tag{6.23}$$

so that we can write

$$Z_{3d} \geqslant \sum_{3-\text{colourings}} 2^{3m_1-4i_1} = \sum_{W \text{ link config.}} 2^{3m_1} \sum_{B,R \text{ links}} 2^{-4i_1} \tag{6.24}$$

where we simply separate the sum over the admissible W links from that over the B and R links along BR loops. Since the m_1 BR loops can be chosen to be direct or indirect independently, the latter sum factorises and contributes for

$$\sum_{i_1=0}^{m_1} \binom{m_1}{i_1} \frac{1}{2^{4i_1}} = \left(1 + \frac{1}{2^4}\right)^{m_1} = (17/16)^{m_1}, \tag{6.25}$$

and hence we finally get

$$Z_{3d} \geqslant \sum_{W \text{ links}} (17/2)^{m_1}. \tag{6.26}$$

According to Eq. (6.14), the latter partition sum is nothing but that of 2d folding in staggered magnetic field h_{st}^{**}, such that

$$2\cosh 6h_{st}^{**} = \tfrac{17}{2}, \tag{6.27}$$

i.e.

$$h_{st}^{**} = \frac{1}{6} \ln \frac{17 + \sqrt{273}}{4}. \tag{6.28}$$

This gives the following lower bound on q_{3d}:

$$q_{3d} \geqslant q_{2d}(h_{st}^{**}) = 1.4351799\ldots. \tag{6.29}$$

Comparing this bound with the numerical estimate (5.8), we suspect that the exact result for q_{3d} differs from this value by no more than 1 percent.

We can also obtain a majoration of Z_{3d} by use of the Hölder inequality on averages, namely

$$\langle A \times B \times C \rangle \leqslant \langle A^\alpha \rangle^{1/\alpha} \langle B^\beta \rangle^{1/\beta} \langle C^\gamma \rangle^{1/\gamma}, \tag{6.30}$$

where $1/\alpha + 1/\beta + 1/\gamma = 1$. The majoration reads

$$\begin{aligned} Z_{3d} &= \sum_{3-\text{colourings}} 2^{m_1} \times 2^{m_2} \times 2^{m_3} \\ &\leqslant \left(\sum_{3-\text{colourings}} 2^{\alpha m_1} \right)^{1/\alpha} \left(\sum_{3-\text{colourings}} 2^{\beta m_2} \right)^{1/\beta} \left(\sum_{3-\text{colourings}} 2^{\gamma m_3} \right)^{1/\gamma}. \end{aligned} \tag{6.31}$$

The 3 terms on the r.h.s. of (6.31) are readily identified as powers of 2d folding partition sums (6.14) with respective staggered magnetic fields

$$h_{st}(x) = \tfrac{1}{6} \ln(2^x + \sqrt{2^{2x} - 1}), \quad x = \alpha, \beta, \gamma. \tag{6.32}$$

The lowest upper bound provided by (6.30) corresponds in fact to $\alpha = \beta = \gamma = 3$, which leads to

$$q_{3d} \leqslant q_{2d}(h_{st}(3)) = 1.589469\ldots. \tag{6.33}$$

7. Discussion

7.1. Estimating q_{3d}

In our strategy for getting lower bounds on q_{3d}, we first considered the contribution of a particular state, the ground state of Fig. 14. In this state, the W links form a regular hexagonal pattern, and the $m_1 = N_\Delta/6$ BR loops are all direct. This leads to the first estimate $\sqrt{2}$ of Eq. (6.5). Keeping the W links fixed, elementary excitations are obtained by exchanging the B and R links along some loops, thus reversing their orientation from direct to indirect. As shown in Appendix A, these excitations have a fugacity $1/2^4$ along with some interactions. Ignoring the interactions leads to the improved lower bound $\sqrt{2}(1 + 1/2^4)^{1/6}$ (A.3). Taking these interactions into account leads to the lower bound q_{BR} of (A.5), expressed in terms of the entropy of a loop gas on the hexagonal lattice, reproducing the high-temperature expansion of the O($n = 4$) model at coupling $K = \frac{1}{2}$ (A.8).

In parallel, we also considered the sum over all admissible configurations of W links. With all BR loops direct, we get the first estimate $q_{2d}(h_{st}^*)$ of Eq. (6.22), with $2\cosh 6h_{st}^* = \sqrt{2}^6$. For each W link configuration, elementary excitations also correspond to reversing the orientation of some BR loops from direct to indirect. There also, we were led to assign a weight $1/2^4$ per indirect loop (see (6.24)), and we obtained the bound $q_{2d}(h_{st}^{**})$ of Eq. (6.29) with $2\cosh 6h_{st}^{**} = \left(\sqrt{2}(1 + 1/2^4)^{1/6}\right)^6$. It is therefore tempting to conjecture the lower bound

$$q_{3d} \geqslant q_{2d}(h_{st}^{***}) \tag{7.1}$$

with

$$2\cosh 6h_{st}^{***} = (q_{BR})^6 \tag{7.2}$$

to account for interactions between the indirect loops, with q_{BR} given by (A.8). This lower bound could in fact be the exact value of q_{3d} since it would incorporate all the effects of excitations. q_{BR} is estimated through a Mayer expansion in Eq. (A.4). With this estimation, we get

$$q_{2d}(h_{st}^{***}) \sim 1.4356\ldots. \tag{7.3}$$

7.2. d-dimensional generalisation

The 3d octahedral folding problem has a natural generalisation to $\mathbb{R}^d$, by considering folding on a generalised d-dimensional FCC lattice. Equivalently, this is done by restricting the d-dimensional tangent vectors to be the edges of the oriented polytope of $\mathbb{R}^d$ generalising the octahedron, whose $2 \times d$ vertices have positions $\pm e_i/\sqrt{2}$, where e_i, $i = 1, \ldots, d$ is the canonical basis of $\mathbb{R}^d$. The $2d(d-1)$ unit tangent vectors read $\epsilon_i x_i + \epsilon_j x_j$ ($x_i = e_i/\sqrt{2}$ as before). They form $4d(d-1)(d-2)/3$ triplets with vanishing sum, corresponding to the faces of the polytope. This gives $3! \times 4d(d-1)(d-2)/3 =$

$8d(d-1)(d-2)$ possible environments for a given triangle. Any such environment still takes the form displayed in Fig. 12, where now $1 \leqslant i \neq j \neq k \leqslant d$. As in the 3d case, let us consider the tangent vectors as link variables on the dual hexagonal lattice. The tangent vectors with non-zero x_i component form m_i loops along which the sign ϵ_i alternates, for $i = 1, \ldots, d$. These loops form a *dense* covering of the hexagonal lattice in the following way: any vertex of the hexagonal lattice belongs to exactly three loops of different type, and any link of the hexagonal lattice belongs to exactly two loops of different type. As in the 3d case, the two choices of ϵ_i signs per loop lead to a partition function

$$Z_d = \sum_{\text{dense loops}} 2^{m_1+m_2+\ldots+m_d}. \tag{7.4}$$

To compute the number of possible vertex environments, we evaluate the partition function of a single hexagon H with external legs (as in (6.2))

$$\begin{aligned} Z_{d,H} &= \sum_{\substack{\text{dense loops} \\ \text{on } H}} 2^{m_1+\ldots+m_d} \\ &= 2^7 r_d + 2^6 s_d, \end{aligned} \tag{7.5}$$

where r_d (resp. s_d) denotes the number of configurations with (resp. without) an internal closed loop: the first term corresponds to 7 loops (1 closed internal loop and 6 open loops entering and exiting the hexagon through the external legs), whereas the second only has a total number of 6 loops. Let us first compute the number r_d of configurations with a closed internal loop. We fix the type of the central loop, say to x_1 (among the d possible choices). Around each vertex of the hexagon, as the x_1 loop occupies the two inner (left and right) links, the only possibility is that a loop of type x_i occupies the left and external links, whereas a loop of type x_j occupies the right and external links, with $2 \leqslant i \neq j \leqslant d$. This suggests the introduction of a transfer matrix $M^{(0)}$ of size $(d-1) \times (d-1)$ mapping an internal link to the subsequent one, with entries

$$M^{(0)}_{i,j} = (1 - \delta_{i,j}), \quad 2 \leqslant i, j \leqslant d. \tag{7.6}$$

We find

$$r_d = d \operatorname{Tr}\left[M^{(0)}\right]^6 = d(d-2)\left((d-2)^5 + 1\right), \tag{7.7}$$

where the prefactor d accounts for the d possible choices of the type of the internal loop. Next let us evaluate the total number $r_d + s_d$ of loop configurations on H. Here again, we need to construct a transfer matrix from an internal link to the subsequent one. The state of a link is specified by the two types $i < j$ of loops to which it belongs, namely $\frac{1}{2}d(d-1)$ choices. The desired transfer matrix has therefore the size $\frac{1}{2}d(d-1) \times \frac{1}{2}d(d-1)$, and its entries read

$$M_{ij;kl} = \delta_{ik}(1 - \delta_{jl}) + \delta_{jl}(1 - \delta_{ik}) + \delta_{il} + \delta_{jk} \tag{7.8}$$

for $1 \leqslant i < j \leqslant d$ and $1 \leqslant k < l \leqslant d$. Note that this matrix is slightly different from that used for the 3d folding problem (4.3). After some algebra, we find

$$r_d + s_d = \mathrm{Tr} M^6 = d(d-1)(d-2)(d^4 + 42d^3 - 380d^2 + 1096d - 1072). \quad (7.9)$$

Using (7.7) and (7.5), we finally get

$$Z_{\mathrm{d,H}} = 64d(d-1)(d-2)(2d^4 + 33d^3 - 349d^2 + 1047d - 1041). \quad (7.10)$$

Factoring out the $8d(d-1)(d-2)$ configurations of a given triangle, the d-dimensional folding problem is therefore equivalent to a V_d-vertex model, with

$$V_d = 8(2d^4 + 33d^3 - 349d^2 + 1047d - 1041). \quad (7.11)$$

We recover $V_3 = 96$ for the 3d folding problem, whereas $V_4 = 1496$, $V_5 = 6752$, $V_6 = 19176\ldots$.

8. Conclusion

In this paper, we have defined the 3d octahedral folding i.e. the folding of the triangular lattice on the 3d FCC lattice. This model was formulated as a 96-vertex model, with two face spin variables z and σ subject to the two folding rules (4.9), (4.13). Equivalently, the partition function of this model was re-expressed as that of a dressed 3-colouring problem, involving a dense covering of the hexagonal lattice by bi-coloured loops. With these two formulations at hand, we were able to estimate the folding entropy $s_{3\mathrm{d}} = \ln q_{3\mathrm{d}}$, both numerically by use of a transfer matrix and analytically by deriving various exact bounds.

Beyond mere counting of folding states, it would be interesting to obtain the complete phase diagram of this system, including both bending rigidity and magnetic field as was performed in Ref. [15] for the 2d case. In particular, it would be desirable to know the precise status of the crumpling transition in this framework, including its order (first or second).

Acknowledgements

The research of M.B. was supported by the Department of Energy, USA, under contract No. DE-FG02-85ER40237. M.B. and E.G. are also grateful for support under NSF grant No. PHY89-04035 from the Institute for Theoretical Physics at Santa Barbara, where this work was initiated. We thank J.-M. Normand for a critical reading of the manuscript.

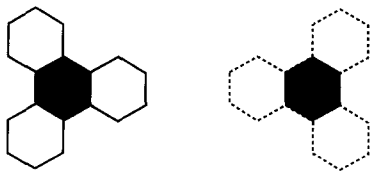

Fig. A.1. An elementary BR excitation of the antiferromagnetic ground state of Fig. 14. The B and R links are exchanged on the shaded hexagon. The three neighbouring BW hexagons are glued to form one loop (thick solid line on the first figure), whereas similarly the three neighbouring WR hexagons are glued to form one loop (thick dashed lines on the second figure).

Appendix A

Lower bounds on the entropy from local excitations

Starting from the fundamental colouring state of Fig. 14, we consider the following local excitation: pick a particular BR hexagon, and exchange its B and R links. The effect of a BR excitation on the neighbouring BW and WR loops is illustrated in Fig. A.1. In this new colouring configuration, m_1 is clearly unchanged, but the three BW neighbouring hexagons have been glued into just one loop (thick solid line on Fig. A.1), hence m_2 is decreased by 2, and the same applies to the three WR neighbouring hexagons (thick dashed line in Fig. A.1), hence m_3 is also decreased by 2. Therefore the total weight of the excited configuration is

$$2^{N_\Delta/2-4}. \tag{A.1}$$

Now there may be any number of BR local excitations in the system, but their interactions will result in a modification of their weight. The number of loops can only be increased by such interactions however, as will become clear below. From now on, we factor out the term $\sqrt{2}^{N_\Delta}$ in the partition function. The above leads to a lower bound for Z_{3d} by considering a non-interacting gas of BR excitations with fugacity $1/2^4$, taking place among the $N_H/3$ hexagons of BR type, with partition function

$$Z_{BR}^{(0)} = 2^{N_\Delta/2} \times \left(1 + \frac{1}{2^4}\right)^{N_H/3} = \left(\frac{17}{2}\right)^{N_\Delta/6}. \tag{A.2}$$

Hence the improved lower bound on q_{3d}

$$q_{3d} \geqslant \left(\tfrac{17}{2}\right)^{1/6} = 1.4285\ldots. \tag{A.3}$$

The BR excitations take place on the BR hexagons of the fundamental state of Fig. 14, i.e. on the vertices of a triangular lattice of larger size, which we call the excitation lattice from now on. Excitations which are not neighbours on this lattice do not interact, namely their total weight factorises into the product of their individual weights. In fact, there is no two-body interaction between them: when two such excitations are neighbours as illustrated in Fig. A.2, i.e. only connected by a W link, the total number of loops is reduced by 8 (five neighbouring BW hexagons are glued into one loop,

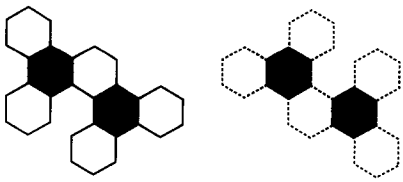

Fig. A.2. Two neighbouring BR excitations. The BR excitations take place on the shaded hexagons. The first figure shows how five former BW hexagons have been glued into a single loop (thick solid line) leading to $m_2 \to m_2 - 4$. The second figure shows how five former WR hexagons have been glued into a single loop (thick dashed line) leading to $m_3 \to m_3 - 4$.

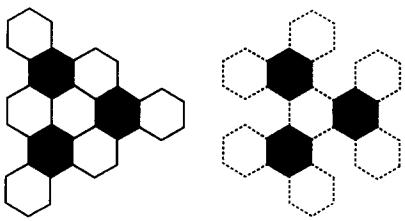

Fig. A.3. Three neighbouring BR excitations. The picture on the left shows how the 6 former neighbouring BW hexagons have been glued to form two loops (thick solid lines) leading to $m_2 \to m_2 - 4$. The picture on the right shows how the 7 neighbouring WR hexagons have been glued to form a single loop (thick dashed line) leading to $m_3 \to m_3 - 6$. The total number of loops is therefore decreased by $10 = 12 - 2$, showing that the three-body interaction weight is 2^2. Note the asymmetry between BW and WR loops.

hence $m_2 \to m_2 - 4$, and five neighbouring WR hexagons are glued into one loop, hence $m_3 \to m_3 - 4$); hence a relative weight $1/2^8 = 1/2^4 \times 1/2^4$.

There is, however, a non-trivial three-body interaction, when three BR excitations take place on the three BR neighbours of a BW or a WR hexagon, as depicted in Fig. A.3. Indeed, the three excitations re-create a central loop with B and R exchanged, thus increasing the total number of loops. A more precise counting (see Fig. A.3) shows in this case that the total number of loops is increased by 2 (only 10 loops have disappeared, instead of $12 = 3 \times 4$ for three independent excitations), resulting in a three-body interaction weight 2^2. The partition function Z_{BR} incorporating any BR excitation can be evaluated order by order in the number of BR excitations. At this stage, the lower bound (A.3) can therefore still be improved by performing a Mayer expansion of the free energy per hexagon, in increasing order of the number of BR excitations. Up to order 5 in the number of BR excitations, we find the partition function per hexagon

$$(q_{BR})^6 = 8\left(1 + \frac{1}{2^4} + \frac{3}{2^{11}} + \frac{3}{2^{13}} + \frac{69}{2^{19}} + \dots\right) \geqslant 8 \times 1.0644\dots, \tag{A.4}$$

hence the improved lower bound

$$q_{3d} \geqslant q_{BR} \geqslant 1.429\dots. \tag{A.5}$$

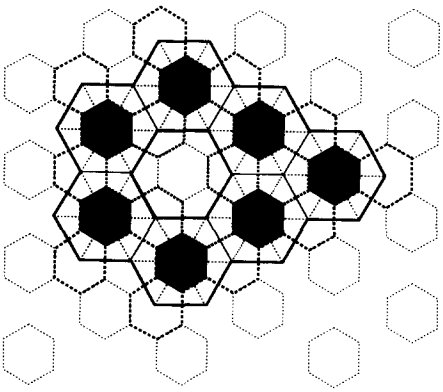

Fig. A.4. A typical cluster of BR excitations. The BR hexagons are represented by thin dotted lines: their centers sit at the vertices of a triangular lattice. The shaded hexagons are excited, namely their B and R links are exchanged. The two-component thick solid line is the boundary of the cluster, drawn on the links of the original triangular lattice (thin dotted lines). The 3 loops in thick dashed lines result from the gluing of the BW hexagons touching the boundary of the cluster. This reduces number of BW loops $m_2 \to m_2 - 10$. The WR loops have not been represented for simplicity. The reader will convince himself that their number is reduced by the cluster to $m_3 \to m_3 - 12$. On the other hand, the two connected components of the boundary have respective lengths 6 and 20, satisfying $(6-2)+(20-2) = 10+12$, as expected.

Let us finally show that the contribution Z_{BR} to the partition function of the most general combination of BR excitations of the above ground state is directly expressible as the high-temperature expansion of a particular O(n) model on the hexagonal lattice. Indeed, any combination of excitations can be decomposed into *clusters* which do not interact with each other. A typical cluster of BR excitations is shown in Fig. A.4: the BR hexagons are represented by thin dotted lines; the excited BR hexagons (i.e. with B and R links exchanged) forming the cluster are shaded. Note that the W links stay in the initial state of Fig. 14, as they are not affected by BR excitations. The clusters are indeed clusters of neighbouring vertices on the excitation lattice. The dual white links form an hexagonal sublattice of the original triangular lattice, which is also the dual of the excitation lattice. We define the *boundary* of a given cluster as its envelope of W links on this lattice (the boundary does not include internal W links which separate neighbouring BR excitations in the cluster). The boundary of the cluster is represented in Fig. A.4 by thick solid lines: note that the boundary links (which are W links of the original triangular lattice) cut white links of former BW or WR hexagons, which are glued together by the BR excitation. A given cluster C receives the relative weight

$$\prod_{\substack{\text{boundary}\\ \text{components}}} \prod_{\substack{\text{connected}\\ c}} 2^{2-\ell_c}, \tag{A.6}$$

where the product extends over all the connected components c of the boundary of the cluster (there are two such components for the boundary of the cluster of Fig. A.4). The number ℓ_c denotes the total length of the connected component c, namely the total number of W links forming c (the two corresponding lengths are 6 and 20 for the

example of Fig. A.4).

This result can be easily understood qualitatively. In the bulk inside a cluster, the hexagonal loops of BW and WR type are simply exchanged. Therefore, the changes in the numbers of loops can only take place at the boundary of the cluster, where some BW (resp. WR) hexagons are glued together to form larger loops, thus decreasing the values of m_2 (resp. m_3).

Eq. (A.6) can be proved by recursion, by studying the effect of adding an extra BR excitation to a given cluster C. Of course (A.6) holds for a single isolated BR excitation, in which case $\ell_c = 6$, and we recover the individual weight $1/2^4$ (A.1).

Notice now that the weight (A.6) only depends on the boundaries of the clusters, which form a set of loops drawn on the white links of the ground state of Fig. 14. This leads to a re-expression of the partition function Z_{BR} for all possible BR excitations as that of a loop gas on this (original W links) hexagonal lattice

$$Z_{BR} = 2^{N_\Delta/2} \sum_{\substack{\text{loops on the} \\ \text{hexag. latt.}}} \prod_{\text{loops}} 2^{2-\ell}, \tag{A.7}$$

where ℓ denotes the length of each loop. The sum in Eq. (A.7) is nothing but the high-temperature expansion of the O(n) model of Ref. [18] on the hexagonal lattice, with $n = 4$ and $K = \frac{1}{2}$. Hence

$$q_{BR} = \sqrt{2}\left(q_{\mathrm{O}(n=4)}(K = \tfrac{1}{2})\right)^{1/6}, \tag{A.8}$$

where $q_{\mathrm{O}(n)}(K)$ denotes the thermodynamic partition function per hexagon of the O(n) model. Unfortunately the partition function for the O($n = 4$) model is not known exactly. The model can be mapped [18] onto a 6-vertex model on the Kagomé lattice, whose vertices sit at the center of the links of the hexagonal lattice. The latter however is a 6-vertex model *in a magnetic field*, for which no exact solution is available. Nevertheless, the Mayer expansion above (A.4) is expected to converge rapidly, and the value found for the lower bound should be accurate to the first three digits (the order 5 term in the expansion is only $\sim 10^{-4}$).

Still q_{BR} as given by (A.8) is only a lower bound on $q_{3\mathrm{d}}$.

References

[1] D.R. Nelson, T. Piran and S. Weinberg, eds., Statistical mechanics of membranes and surfaces, Proc. 5th Jerusalem Winter School for theoretical physics (World Scientific, Singapore, 1989).

[2] D.R. Nelson and L. Peliti, J. Phys. France 48 (1987) 1085.

[3] M. Paczuski, M. Kardar and D.R. Nelson, Phys. Rev. Lett. 60 (1988) 2638.

[4] F. David and E. Guitter, Europhys. Lett. 5 (1988) 709.

[5] Y. Kantor and D.R. Nelson, Phys. Rev. Lett. 58 (1987) 2774; Phys. Rev. A 36 (1987) 4020.

[6] Y. Kantor, M. Kardar and D.R. Nelson, Phys. Rev. Lett. 57 (1986) 791; Phys. Rev. A 35 (1987) 3056;
M. Baig, D. Espriu and J. Wheater, Nucl. Phys. B 314 (1989) 587;
J. Ambjørn, B. Durhuus and T. Jonsson, Nucl. Phys. B 316 (1989) 526;
R. Renken and J. Kogut, Nucl. Phys. B 342 (1990) 753;
R. Harnish and J. Wheater, Nucl. Phys. B 350 (1991) 861;

J. Wheater and P. Stephenson, Phys. Lett. B 302 (1993) 447;
M. Baig, D. Espriu and A. Travesset, Nucl. Phys. B 426 (1994) 575.
[7] J.A. Aronovitz and T.C. Lubensky, Phys. Rev. Lett. 60 (1988) 2634;
E. Guitter, F. David, S. Leibler and L. Peliti, Phys. Rev. Lett. 61 (1988) 2949; J. Phys. France 50 (1989) 1787;
J.A. Aronovitz, L. Golubovic and T.C. Lubensky, J. Phys. France 50 (1989) 609;
F.F. Abraham and D.R. Nelson, Science 249 (1990) 393;
C.F. Schmidt et al., Science 259 (1993) 952.
[8] M. Kardar and D.R. Nelson, Phys. Rev. Lett. 58 (1987) 1289, 2280 (E); Phys. Rev. A 38 (1988) 966;
J.A. Aronovitz and T.C. Lubensky, Europhys. Lett. 4 (1987) 395;
B. Duplantier, Phys. Rev. Lett. 58 (1987) 2733; 62 (1989) 2337;
B. Duplantier, T. Hwa and M. Kardar, Phys. Rev. Lett. 64 (1990) 2022;
T. Hwa, Phys. Rev. A 41 (1990) 1751;
F. David, B. Duplantier and E. Guitter, Phys. Rev. Lett. 70 (1993) 2205; Nucl. Phys. B 394 (1993) 555; Phys. Rev. Lett. 72 (1994) 311.
[9] M. Plischke and D. Boal, Phys. Rev. A 38 (1988) 4943;
F.F. Abraham, W.E. Rudge and M. Plischke, Phys. Rev. Lett. 62 (1989) 1757;
D. Boal, E. Levinson, D. Liu and M. Plischke, Phys. Rev. A 40 (1989) 3292;
J.-S. Ho and A. Baumgärtner, Phys. Rev. Lett. 63 (1989) 1324;
Z. Zhang, H. Davis and D. Kroll, Phys. Rev. E 48 (1993) R651.
[10] G. Grest, J. Phys. I France 1 (1991) 1695.
[11] A. Baumgärtner and W. Renz, Europhys. Lett. 17 (1992) 381.
[12] Y. Kantor and M.V. Jarić, Europhys. Lett. 11 (1990) 157.
[13] P. Di Francesco and E. Guitter, Europhys. Lett. 26 (1994) 455.
[14] R.J. Baxter, J. Math. Phys. 11 (1970) 784; J. Phys. A 19 (1986) 2821.
[15] P. Di Francesco and E. Guitter, Phys. Rev. E 50 (1994) 4418.
[16] D. Shanks, J. Math. Phys. 34 (1955) 1.
[17] C. Brezinski and M. Redivo Zaglia, Extrapolation methods (North-Holland, Amsterdam, 1991).
[18] E. Domany, D. Mukamel, B. Nienhuis and A. Schwimmer, Nucl. Phys. B190 (1981) 279;
B. Nienhuis, Phys. Rev. Lett. 49 (1982) 1062; J. Stat. Phys. 34 (1984) 731.